https://doi.org/10.1051/epjconf/202636800022

Shell-driven mode evolution in the fission of sub-lead nuclei

V. S. Muddam[1,*], J. Buete[1], K. J. Cook[1], D. J. Hinde[1], M. Dasgupta[1], S. L. Hayles[1], H. Lee[1], C. C. Seabra[1], J. A. Stuchbery[1], T. Tran[1], and M. M. Webber[1]

[1]Department of Nuclear Physics and Accelerator Applications, Research School of Physics, Australian National University, Canberra, ACT 2601, Australia

Abstract. Systematic measurements and analysis of the heavy-ion fusion-fission of ^{148,152,154,158}Dy, ^{160,164,168}Yb, and ^{176,178,180,184,186}Pt isotopes are presented, spanning a wide range of neutron-to-proton ratios in the sub-lead region. We reconstruct two-dimensional M_{R}-RTKE distributions and perform a multi-modal Gaussian decomposition to determine the shell effects driving fission fragment formation. All systems exhibit clear evidence of shell-driven fission beyond the liquid-drop mode. A persistent inner asymmetric mode is observed at a fission fragment proton number of $Z = 36$ across all isotopic chains. In addition, Dy and Yb isotopes exhibit an outer asymmetric mode correlated with a fission fragment neutron number of $N = 36$, providing the first experimental evidence for a neutron-driven shell gap influencing fission below lead. These results demonstrate that multiple microscopic shell structures, both proton and neutron, coexist and influence fission fragment formation across isotopic chains in the sub-lead region.

1 Introduction

Nuclear fission is a complex and dynamic quantum many-body process that involves the large deformation of a nucleus before it splits into two fragments. Although discovered 87 years ago [1], a central challenge has been understanding the distribution of fragment masses produced when a nucleus splits. In the actinide region, experiments since the discovery of fission have established that low-energy fission is strongly mass asymmetric, with a pronounced heavy-fragment peak near $A \approx 140$ [2, 3]. This behaviour is now thought [4] to arise from octupole-deformed shell gaps that favour the formation of fragments with proton numbers $Z = 52$ to $Z = 56$. These fragment shells stabilise asymmetric splits across many actinide nuclides.

By contrast, lighter systems in the sub-lead region were historically expected to fission symmetrically, producing two fragments of nearly equal mass [3]. This picture changed dramatically when a series of experiments demonstrated clear asymmetric mass splits in nuclei far below the actinides [5–9]. The landmark experiment was the fission of the sub-lead nucleus ^{180}Hg, which exhibited peaks near $A = 80$ and $A = 100$ [5, 10], corresponding to fragments with proton numbers $Z \approx 36$ and/or $Z \approx 44$. The observation of asymmetric fission in ^{180}Hg suggested that new shell gaps, distinct from those in the actinides, govern fragment formation in the sub-lead region [11]. This motivated a wide range of experimental and theoretical studies in the sub-lead region.

Recent large-scale investigations have reached differing conclusions about the origin of asymmetry in the sub-lead region. A significant advance came from a recent study that measured over 100 nuclides across a broad range of masses but within a narrow band of elements [12]. Measurements of fragment charge suggested a single dominant proton shell gap at $Z = 36$ (quadrupole-deformed) as the universal driver of asymmetric fission below lead. In contrast, a high-precision study spanning a much wider elemental range, from ^{144}Gd to ^{212}Th, found clear evidence for the coexistence of two quadrupole-deformed proton gaps, near $Z = 34, 36$ and $Z = 44, 46$ [13]. This broader isotopic and elemental coverage revealed systematic transitions between modes, where, notably, the same shell gaps appeared not only at asymmetric mass splits but also at symmetric ones, extending the idea of shell-driven fission. However, both these studies have either examined nuclei with the same N/Z ratio or have measured only fragment charges, leaving the neutron numbers of the fragments undetermined. As a result, the influence of the compound nucleus neutron number on the persistence of shell effects and the extent to which neutron shell gaps influence fission in the sub-lead region remain poorly understood, motivating an investigation of fission across isotopic chains.

In this paper, we present a systematic study of sub-lead fission spanning a wider range of N/Z than previously studied. By measuring fission fragment mass distributions across isotopes of ^{148,152,154,158}Dy, ^{160,164,168}Yb, and ^{176,178,180,184,186}Pt, we track how asymmetric and symmetric fission modes evolve with increasing compound nucleus neutron number, allowing us to understand how multiple shell-driven modes persist across the sub-lead region, and the role of proton and neutron shell gaps in influencing fission below lead.

---

[*] e-mail: vaishnavi.muddam@anu.edu.au

2 Experimental Methods

Fission measurements of ^{148,152,154,158}Dy, ^{160,164,168}Yb, and ^{176,178,180,184,186}Pt were induced using heavy-ion fusion at the Heavy Ion Accelerator Facility at the Australian National University. Pulsed beams of ^{16}O, ^{28,30}Si, and ^{32,34}S were directed from the 14UD tandem accelerator onto targets of ^{116}Sn, ^{124,128}Te, and ^{144,148,152,154}Sm. The targets had areal densities between 20 and 140 μg cm^{-2} and were angled at 60° to the beam. A full list of reactions, and beam, centre-of-mass, and excitation energies is given in Table 1. The produced compound nuclei span N/Z ratios of 1.24 to 1.40, to probe the persistence of shell effects across isotopes of the same element. Quasifission does not contribute significantly as the chosen mass asymmetry of the entrance channel results predominantly in fusion-fission [14].

Fission fragments were detected in coincidence using the CUBE fission spectrometer, consisting of three multi-wire proportional counters (MWPC) configured as shown in Ref. [15]. The mass-ratio of the fission fragments, defined as $M_R = \frac{m_1}{m_1+m_2}$, where $m_{1,2}$ are the masses of the fission fragments, as well as the total kinetic energies (TKE), were determined using the kinematic coincidence method [16]. Although post-scission neutron evaporation does perturb the fragment velocities, these recoils are expected to be isotropic in their centre of mass and therefore broaden the reconstructed mass-ratio distribution without introducing a systematic shift in the mean M_R . This allows M_R to be interpreted as the mass division at scission. Pre-scission neutron evaporation will modify the derived neutron number of the fragments, but for the systems studied here, it is expected to be modest and to vary smoothly across isotopic chains. GEF calculations [17] for Pt isotopes indicate an average pre-scission neutron evaporation of 0.3 neutrons. A much larger average of one neutron being emitted will propagate as a shift of less than 0.5 nucleons in the inferred fission fragment neutron number. As a result, while pre-scission evaporation may introduce a slight systematic offset in the inferred fragment neutron numbers, it does not alter the relative trends or the identification of shell-driven modes that persist across multiple isotopes.

Table 1. Summary of reaction systems studied, showing compound nucleus (CN) charge Z_{CN}, neutron number N_{CN}, beam energy E_{beam}, centre-of-mass energy E_{cm}, and compound nucleus excitation energy E_x above the ground state, where E_{cm} and E_x have been corrected for energy loss through the target.

Reaction	CN	Z_{CN}	N_{CN}	E_{beam} (MeV)	E_{cm} (MeV)	E_x (MeV)
^{32}S + ^{116}Sn	^{148}Dy	66	82	148.0	115.3	65.6
^{28}Si + ^{124}Te	^{152}Dy	66	86	147.0	119.5	77.6
^{30}Si + ^{124}Te	^{154}Dy	66	88	147.0	118.0	73.4
^{30}Si + ^{128}Te	^{158}Dy	66	92	147.0	117.8	74.8
^{16}O + ^{144}Sm	^{160}Yb	70	90	107.0	95.2	66.6
^{16}O + ^{148}Sm	^{164}Yb	70	94	107.0	95.9	72.8
^{16}O + ^{152}Sm	^{168}Yb	70	98	107.0	96.1	78.2
^{32}S + ^{144}Sm	^{176}Pt	78	98	151.0	123.9	44.8
^{34}S + ^{144}Sm	^{178}Pt	78	100	146.0	117.6	37.7
^{32}S + ^{148}Sm	^{180}Pt	78	102	142.0	116.8	45.8
^{32}S + ^{152}Sm	^{184}Pt	78	106	148.0	118.9	55.4
^{32}S + ^{154}Sm	^{186}Pt	78	108	142.0	117.6	57.0

3 Results

3.1 Evidence for Shell-Driven Fission

In the simplest, liquid-drop picture, the fission fragment mass distribution is described by a single Gaussian. Each of the twelve Dy, Yb, and Pt mass distributions (top panels of each row of Figure 1) was fit with a single, symmetric Gaussian. The resulting residuals, defined as the point-by-point difference between the data and the fitted model, show clear systematic deviations (bottom panels of each row of Figure 1). Pt isotopes (top row) show the most pronounced double-peaked shapes in mass with a clear dip at symmetry, consistent with strong asymmetric contributions, as seen in previous studies of Pt isotopes [9]. While Yb isotope mass distributions (middle row) show little structure, we observe a small peak in the residuals at $M_R = 0.5$, corresponding to symmetric splitting, and two dips near $M_R \approx 0.45$ and 0.55 for all three systems. In contrast, the mass distributions of Dy isotopes (bottom row) evolve from flat-topped to centrally peaked distributions with increasing mass number. The systematic evolution of the mass-distribution structure across all twelve isotopes with increasing mass provides the first evidence for a neutron shell–driven fission mode. This interpretation is motivated by the evolution observed along isotopic chains, suggesting sensitivity to neutron number. The residual structure observed across isotopes also demonstrates that a single symmetric component cannot account for the data: all systems require at least one additional, shell-driven asymmetric contribution.

3.2 Shell-Driven Modes in Two-Dimensions

The reconstructed fission observables, M_R and TKE, provide a probe of the shape of the nucleus at scission. More compact shapes at scission correspond to smaller fragment-fragment separations, leading to stronger Coulomb repulsion and larger TKE values. This correlation indicates that fission modes associated with shell-stabilised compact fragments (e.g., near closed shells) typically exhibit higher average TKE. In comparison, modes with elongated fragment configurations yield lower TKE [9, 13]. Since the Coulomb energy scales with fragment charge product, the TKE varies systematically with M_R. It is thus convenient to remove the trivial Coulomb dependence by linearising the TKE to the Coulomb expectation and normalising to the “Viola TKE systematics” [18, 19], defined as

$$\mathrm{TKE_{Viola}} = 0.755\frac{Z_1 Z_2}{A_1^{1/3} + A_2^{1/3}} + 7.3\ \mathrm{MeV}. \quad (1)$$

The ratio of the measured TKE at each M_R to this expected value defines the relative total kinetic energy,

$$\mathrm{RTKE}(M_R) = \frac{\mathrm{TKE}(M_R)}{\mathrm{TKE_{Viola}}(M_R)}. \quad (2)$$

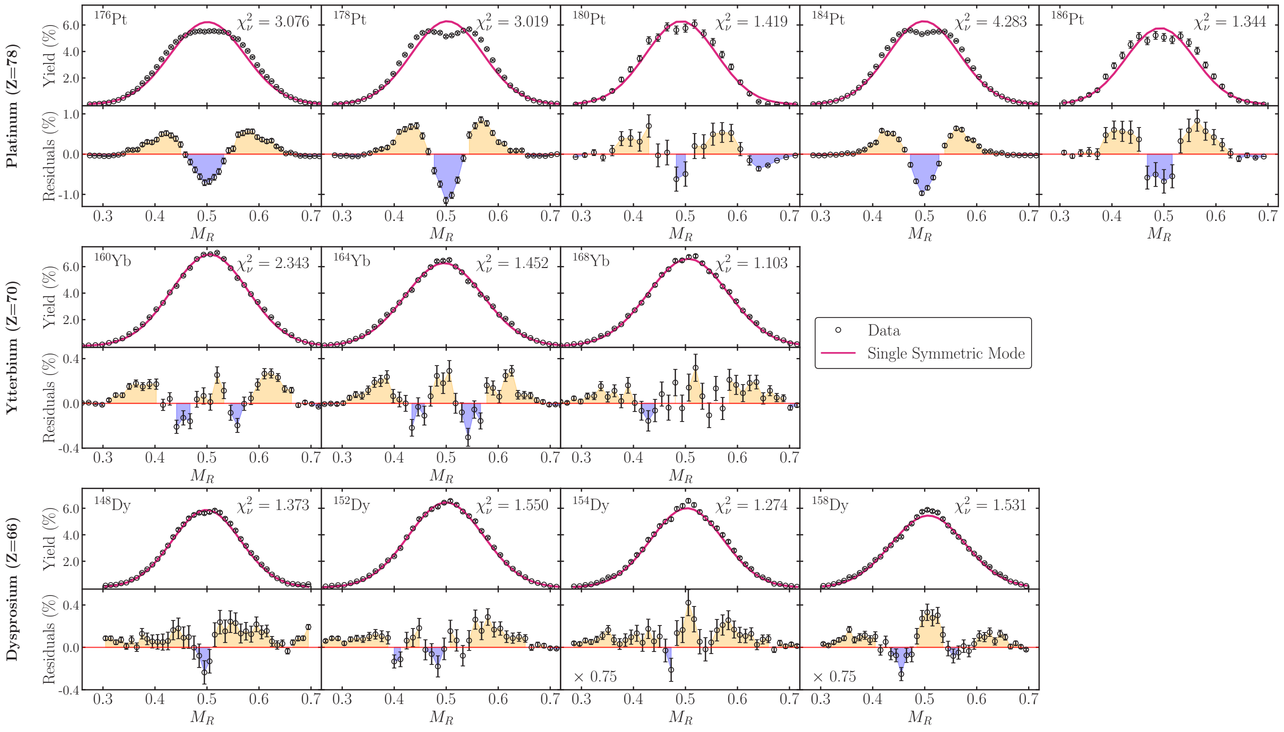

Figure 1. Measured M_{R} distributions for all twelve isotopes of ^{148,152,154,158}Dy, ^{160,164,168}Yb, and ^{176,178}Pt. All distributions are fit with one symmetric mode (shown in pink), with the χ^2_ν shown in the top right of each panel. Deviations from the single Gaussian fits are shown by the residuals at the bottom of each panel. Yellow and blue shading, reflecting positive and negative residuals, respectively, demonstrate that all fissioning systems show evidence of additional fission modes beyond the liquid drop. A scaling factor is shown in the bottom-left corner of some residual panels, allowing common axes.

Shell effects stabilise specific fragment shapes, producing characteristic fission modes that manifest as structures in the M_{R}-RTKE distributions. The task is to decompose these structures into fission modes.

To quantitatively determine the modes, we performed two-dimensional fits in M_{R}-RTKE using the procedure described in Ref. [9]. We represent each fission mode as a 2D Gaussian in the M_{R}-RTKE space, and the sum of all fitted modes gives the total yield. The number of modes required to best reproduce the distribution for each system was found to be one symmetric and two asymmetric modes. This decomposition is consistent with earlier work [9, 13], supporting the presence of two shell-driven asymmetric valleys in addition to the liquid-drop mode. In particular, the asymmetric mode closest to symmetry is recovered at the same centroid regardless of whether the distribution is described by one or two asymmetric components, demonstrating that this solution is not an artefact of the chosen model complexity. Introducing additional modes does not shift the extracted centroids, but instead produces either degenerate components overlapping the established modes or unphysical solutions at the edges of the distributions.

3.3 Shell-Driven Fission Across the Isotopic Chains

The fitted mass centroids were mapped onto fragment proton and neutron numbers using the unchanged-charge-density (UCD) assumption, where the fragments retain the same neutron-to-proton ratio as the compound nucleus [20]. These yield a well-defined (Z, N) centroid for each mode. This mapping is summarised in Figure 2, giving the fission fragment Z_{FF} and N_{FF} as a function of the compound nucleus Z_{CN} and N_{CN}, with coloured bars indicating theoretically predicted deformed shell gaps [4, 11]. We refer to the mode closest to symmetry as the “inner” mode, and to the mode furthest from symmetry as the “outer” mode. Uncertainties are shown as error bars obtained from the covariance matrix returned by the chi-squared fit, where the diagonal elements give the parameter variances.

In all twelve systems, $Z = 36$ consistently appears as a fission fragment in the inner mode [Figure 2(a)]. However, the role played by this shell gap evolves systematically with the mass of the fissioning system. In the Dy isotopes, the $Z = 36$ shell gap corresponds to the heavy fragment, while in the Yb isotopes it lies close to mass symmetry. In the Pt isotopes, by contrast, the same $Z = 36$ shell gap appears as the light fragment. This highlights how the same underlying shell structure manifests differently depending on the mass of the fissioning system. This quadrupole-deformed shell gap [11] is also consistent with shell-driven fission observed in Refs. [12, 13], and is shown here to persist over a larger range of N/Z than previously observed. The corresponding fragment N (Figure 2(b)) largely increases linearly with increasing compound nucleus neutron number for the Dy and Yb iso-

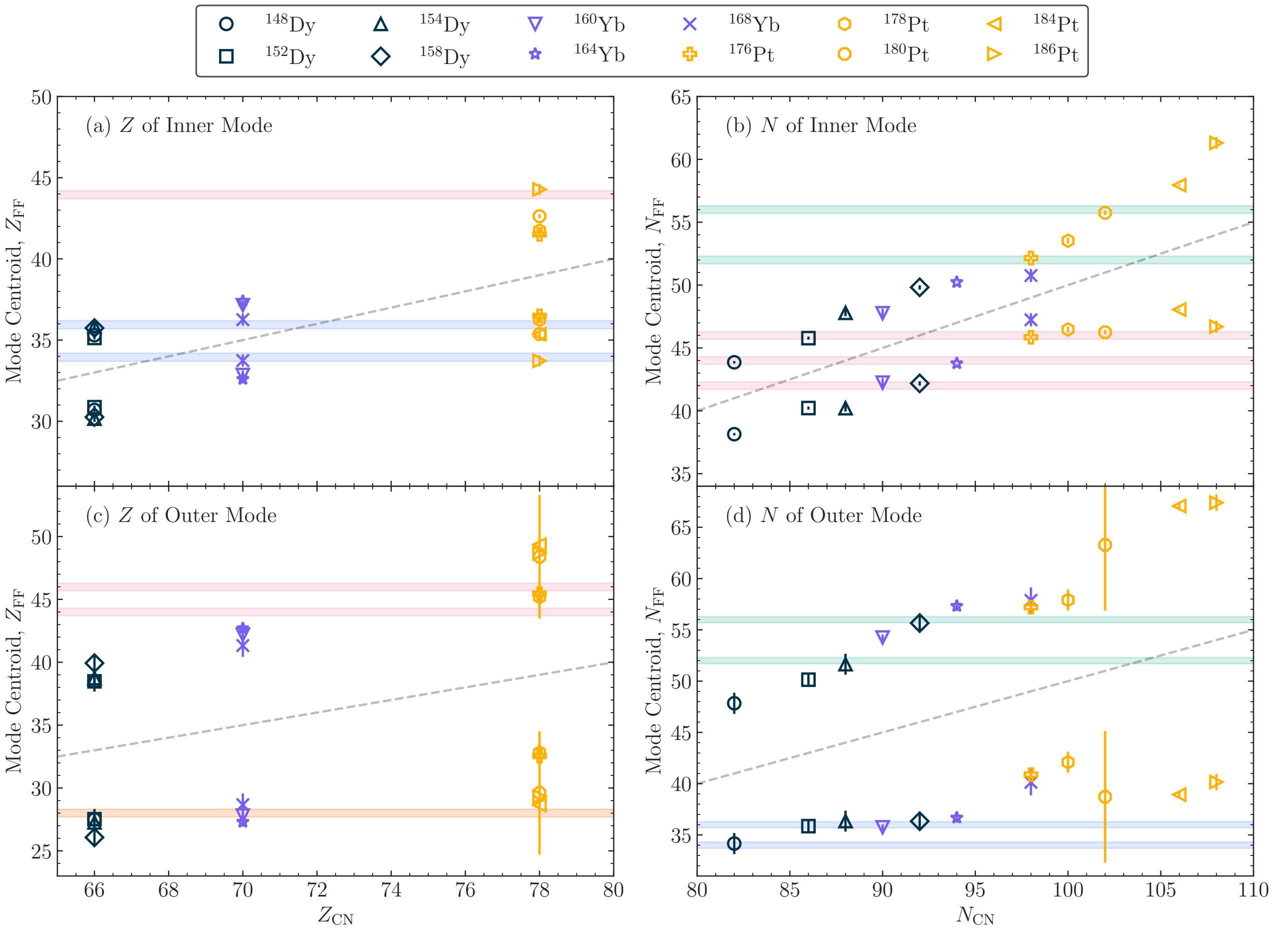

Figure 2. Mode centroids for the inner (panels (a), (b)) and outer (panels (c), (d)) shell-driven fission modes for all twelve isotopes, with uncertainties shown as error bars. The fission fragment proton (Z_{FF}) and neutron (N_{FF}) numbers are given as a function of compound nucleus proton (Z_{CN}) and neutron (N_{CN}) numbers. To guide the eye, the dashed grey line shows the location of mass-symmetric fission. Coloured bars indicate known deformed shell gaps.

topes. In the Pt isotopes, deviations from this trend are observed, with the fragment neutron number showing additional correlation with $N = 46$, suggesting the influence of a competing quadrupole-deformed neutron shell gap in these heavier systems. However, the interpretation of the Pt trends is limited by the reduced statistics available for the heavier isotopes, particularly ^{180}Pt and ^{184}Pt, which introduces larger uncertainties in the fitted centroids and prevents a definitive disentanglement of overlapping shell effects at this stage. Nonetheless, as demonstrated above, the centroid positions are robust to variations in the mode decomposition, supporting their preliminary interpretation even in the lower-statistics Pt systems.

The outer mode centroids, shown in Figure 2(c) and (d), show correlations with both $Z = 28$ and $N = 36$ in Dy and Yb isotopes. However, the slight increase in Z_{FF} with Z_{CN} suggests that it is perhaps the $N = 36$ quadrupole-deformed shell gap that is driving this fission mode in Dy and Yb isotopes. This new neutron-driven mode represents the first experimental observation of such a neutron-driven mode below lead. For ^{168}Yb and ^{176,178}Pt, there is also a correlation with an octupole-deformed neutron shell gap of $N = 56$, which suggests that different shell effects dominate as the mass of the systems increases. For the heavier Pt isotopes, the interpretation of the outer mode centroids is less straightforward. The mode centroids of these heavier isotopes seem to cluster around $N = 40$. However, ^{180}Pt and ^{186}Pt exhibit larger uncertainties and increased scatter in the fitted centroids. This is a direct consequence of the significantly lower statistics available for these systems, which, due to reduced yields and overlapping fission modes, limit the ability to extract mode centroids with greater confidence. As a result, a definitive separation of the competing shell contributions from $Z = 28$ and $N = 40$ in the outer mode for heavier Pt isotopes is not possible with the present data. However, the coexistence of a proton-driven $Z = 36$ inner mode and a neutron-driven $N = 36$ outer mode in Dy and Yb demonstrates that multiple shell gaps simultaneously shape fission, with the same structures influencing fission fragment formation across isotopic chains despite changes in mass.

3.4 Outlook

In summary, these results establish a picture of shell-driven fission in the sub-lead region: a strong proton-driven mode anchored at $Z = 36$ across all twelve isotopes, and a neutron-driven mode anchored at $N = 36$, influencing Dy and Yb isotopes. This marks the first experimental evidence that both proton and neutron shell gaps can act concurrently to shape fission fragment formation in the sub-lead nuclei.

In Pt, the situation is more complex. The inner mode exhibits competing influences from the $Z = 36$ and $N = 46$ gaps, whereas the outer mode overlaps with possible contributions from $Z = 28$, $N = 56$, and $N = 40$, and may involve additional shell gaps. However, the present interpretation is limited by the low statistics available for ^{180}Pt and ^{184}Pt, which prevent a definitive separation of overlapping shell drivers. Future measurements should focus on higher statistics across a broader range of Pt isotopes to stabilise the mode decomposition and to track the evolution of both centroid positions and relative yields with neutron number. In particular, experiments capable of resolving both fragment proton and neutron number will be necessary to disentangle competing proton- and neutron-driven shell effects. Extending such high-statistics isotopic chain measurements to neighbouring elements, such as Gd and Hf, to probe the transition between different shell-driven influences can clarify the persistence, competition, and possible evolution of proton and neutron shell gaps across the wider sub-lead region.

Acknowledgements

This work was supported by Australian Research Council Grants DP200100601, DE230100197, DP230101028, and DP250101791. The authors acknowledge the facilities, and the scientific and technical assistance provided by Heavy Ion Accelerators (HIA). HIA is supported by the Australian Government through the National Collaborative Research Infrastructure Strategy (NCRIS) program. S.L.H., H.L., J.A.S., T.T., and M.M.W acknowledge support from an Australian Government Research Training Program (RTP) Scholarship.

References

[1] L. Meitner et al., Disintegration of Uranium by Neutrons: a New Type of Nuclear Reaction, Nature **143**, 239 (1939). 10.1038/143239a0

[2] C. Böckstiegel et al., Nuclear-fission studies with relativistic secondary beams: Analysis of fission channels, Nuclear Physics A **802**, 12 (2008). 10.1016/j.nuclphysa.2008.01.012

[3] K.H. Schmidt et al., Relativistic radioactive beams: A new access to nuclear-fission studies, Nuclear Physics A **665**, 221 (2000). 10.1016/S0375-9474(99)00384-X

[4] G. Scamps et al., Impact of pear-shaped fission fragments on mass-asymmetric fission in actinides, Nature **564**, 382 (2018). 10.1038/s41586-018-0780-0

[5] A.N. Andreyev et al., New Type of Asymmetric Fission in Proton-Rich Nuclei, Physical Review Letters **105**, 252502 (2010). 10.1103/PhysRevLett.105.252502

[6] B.M.A. Swinton-Bland et al., Mass-asymmetric fission of ^{205,207,209}Bi at energies close to the fission barrier using proton bombardment of ^{204,206,208}Pb, Physical Review C **102**, 054611 (2020). 10.1103/PhysRevC.102.054611

[7] E. Prasad et al., Observation of mass-asymmetric fission of mercury nuclei in heavy ion fusion, Physical Review C **91**, 064605 (2015). 10.1103/PhysRevC.91.064605

[8] E. Prasad et al., Systematics of the mass-asymmetric fission of excited nuclei from ^{176}Os to ^{206}Pb, Physics Letters B **811**, 135941 (2020). 10.1016/j.physletb.2020.135941

[9] B.M.A. Swinton-Bland et al., Multi-modal mass-asymmetric fission of ^{178}Pt from simultaneous mass-kinetic energy fitting, Physics Letters B **837**, 137655 (2023). 10.1016/j.physletb.2022.137655

[10] K. Nishio et al., Excitation energy dependence of fragment-mass distributions from fission of ^{180,190}Hg formed in fusion reactions of ^{36}Ar+^{144,154}Sm, Physics Letters B **748**, 89 (2015). 10.1016/j.physletb.2015.06.068

[11] G. Scamps et al., Effect of shell structure on the fission of sub-lead nuclei, Physical Review C **100**, 041602 (2019). 10.1103/PhysRevC.100.041602

[12] P. Morfouace et al., An asymmetric fission island driven by shell effects in light fragments, Nature **641**, 339 (2025). 10.1038/s41586-025-08882-7

[13] J. Buete et al., Universality of shell effects in fusion-fission mass distributions, Physics Letters B **865**, 139459 (2025). 10.1016/j.physletb.2025.139459

[14] R. Du Rietz et al., Mapping quasifission characteristics and timescales in heavy element formation reactions, Physical Review C **88**, 054618 (2013). 10.1103/PhysRevC.88.054618

[15] T. Banerjee et al., Systematic evidence for quasifission in ^{9}Be−, ^{12}C−, and ^{16}O-induced reactions forming ^{258,260}No, Phys. Rev. C **102**, 024603 (2020). 10.1103/PhysRevC.102.024603

[16] D.J. Hinde et al., Conclusive evidence for the influence of nuclear orientation on quasifission, Physical Review C **53**, 1290 (1996). 10.1103/PhysRevC.53.1290

[17] K.H. Schmidt et al., General Description of Fission Observables: GEF Model Code, Nuclear Data Sheets **131**, 107 (2016). 10.1016/j.nds.2015.12.009

[18] V.E. Viola et al., Systematics of fission fragment total kinetic energy release, Physical Review C **31**, 1550 (1985). 10.1103/PhysRevC.31.1550

[19] D.J. Hinde et al., Neutron emission as a probe of fusion-fission and quasifission dynamics, Physical Review C **45**, 1229 (1992). 10.1103/PhysRevC.45.1229

[20] A.C. Wahl et al., Nuclear-Charge Distribution in Low-Energy Fission, Physical Review **126**, 1112 (1962). 10.1103/PhysRev.126.1112